INTERNATIONAL JOURNAL FOR NUMERICAL METHODS IN FLUIDS
Int. J. Numer. Meth. Fluids **28**: 633–661 (1998)

FREE CONVECTION HEAT TRANSFER FROM AN ISOTHERMAL WAVY SURFACE IN A POROUS ENCLOSURE

B.V. RATHISH KUMAR*, P.V.S.N. MURTHY AND P. SINGH

Department of Mathematics and Scientific Computing, Indian Institute of Technology, Kanpur 208016, India

SUMMARY

The coupled streamfuction–temperature equations governing the Darcian flow and convection process in a fluid-saturated porous enclosure with an isothermal sinusoidal bottom sun face, has been numerically analyzed using a finite element method (FEM). No restrictions have been imposed on the geometrical non-linearity arising from the parameters like wave amplitude (a), number of waves per unit length (N), wave phase (ϕ), aspect ratio (A) and also on the flow driving parameter Rayleigh number (Ra). The numerical simulations for varying values of Ra bring about interesting flow features, like the transformation of a unicellular flow to a multicellular flow. Both with increasing amplitude and increasing number of waves per unit length, owing to the shift in the separation and reattachment points, a row–column pattern of multicellular flow transforms to a simple row of multicellular flow. A cycle of n celluar and $n+1$ cellular flows, with the flow in adjacent cells in the opposite direction, periodically manifest with phase varying between 0 and 360°. The global heat transfer into the system has been found to decrease with increasing amplitude and increasing number of waves per unit length. Only marginal changes in the global heat flux are observed, either with increasing Ra or varying ϕ. Effectively, sinusoidal bottom surface undulations of the isothermal wall of a porous enclosure reduces the heat transfer into the system.

KEY WORDS: free convection; porous enclosure; Darcian model; wavy surface; finite element method; numerical study

1. INTRODUCTION

The study of natural convection in porous enclosures has generated great interest among researchers due to its significance in several scientific and engineering applications, e.g. thermal insulation, geothermal reservoirs, nuclear waste management, grain storage, etc. In building sciences and thermal insulation engineering, an appreciable insulating effect was derived by placing porous material in the gap between the cavity walls and in multishield structures of nuclear reactors between the pressure vessel and the reactor, respectively. Geophysical applications include modeling the spreading of pollutants (e.g. radio nuclides), water movements in geothermal reservoirs, enhanced recovery of petroleum reservoirs (Vafai and Haung [1]), etc.

---

* Correspondence to: Department of Mathematics and Scientific Computing, Indian Institute of Technology, Kanpur 208016, India.

CCC 0271–2091/98/140633–29$17.50

Received June 1996
Revised February 1997

Works by Chan *et al.* [2]; Holst and Aziz [3]; Burns *et al.* [4]; Walker and Homsy [5]; Bejan and Tien [6]; Hickox and Gartling [7]; Prasad and Kulacki [8]; Chang [9]; Bradean and Ingham [10]; Hetsroni *et al.* [11], etc., contribute to the understanding of the convection in porous enclosures.

Enclosure-related studies may be classified into two broad categories, *viz.* enclosures heated from the side and enclosures heated from below. Various flow patterns are possible; depending on the imposed thermal boundary conditions, aspect ratio and the geometry of the enclosures. A comprehensive review of these studies has been given by Meld and Bejan [12]. These studies are largely centered on convection from plane surfaces of rectangular porous enclosures. In practise, one would encounter roughened surfaces in several technological applications, e.g. solar collectors, condensers in refrigerators, etc. Large scale non-uniformities are encountered in grain storage containers, electron circuits dissipating heat (Bhavnani and Bergles [13]; Rees and Pop [14,15]). In fact, in the above and in many other applications, surfaces are intentionally roughened by the attachment of baffles, fins or other suitable protrusions to the walls of the enclosures to affect the heat transfer (Riley [16]; Moulic and Yao [17]). Therefore, it is essential to understand the effect of surface non-uniformities on convective flow and heat transfer. Bhavnani and Bergles [13] give a literature review on free convective heat transfer from non-uniform vertical surfaces in Newtonian fluids. By approximating the small scale roughness as periodic functions, Yao [18]; Watson and Poots [19]; Vajravelu and Sastri [20]; Moulic and Yao [17], etc., have studied free convection in Newtonian fluids. Studies of Yao [18] and those of Moulic and Yao [17] indicate a decrease in total Nusselt number when compared with the flat-wall case despite an increase in the surface area.

The only known papers to date which consider the effects of surface non-uniformities on convection in porous media are those of Rees and Pop [14,15] and Riley [16]. Riley [16] analyzed the effect of surface undulations approximated with cosine waves in the vertical porous slot and his results are confined to the conduction zone only. Rees and Pop [14,15] analyzed natural convection induced by semi-infinite vertical and horizontal wavy surfaces in saturated porous medium under boundary layer approximations. The current literature indicates that no attempt has been made to understand the effects of surface roughness on convection from below in a porous enclosure.

As a first step in this direction, the simulation of flow structure and the natural convection due to a uniformly heated horizontal wavy wall in a saturated porous enclosure is attempted by this paper. The wavy wall is assumed to be sinusoidal in structure. The numerical simulation is carried out by using Bubnov–Galerkin's finite element method (FEM) [21]. The computational experiments are carried out for various values of the parameters and it is observed that, unlike in the boundary layer flow [14], the global heat flux decreases with increasing values of amplitude. The flow driving buoyancy force is seen to enhance the heat transfer into the system, and at the same time, the intensified stream inside the separated region is seen to trap the heat and hinder the heat transfer. Because of this, only marginal changes could be seen in the heat transfer results with the increasing Rayleigh number. The comparison of the heat flux from a wavy surface with that from a flat surface clearly shows that surface undulations decrease the heat flux into a porous enclosure. Interesting patterns of multicellular flow zones are seen to manifest for various values of Ra, a, ϕ and N. These results, together with the global heat flux profiles and isotherms, are clearly depicted through the computer generated plots.

2. GOVERNING EQUATIONS

The conservation equations for mass, momentum and energy for steady two-dimensional flow in an homogeneous and isotropic porous medium are

$$\frac{\partial u}{\partial x}+\frac{\partial v}{\partial y}=0, \tag{1}$$

$$u=-\frac{K}{\mu}\left(\frac{\partial p}{\partial x}\right), \tag{2}$$

$$v=-\frac{K}{\mu}\left(\frac{\partial p}{\partial y}+\rho g\right), \tag{3}$$

$$u\frac{\partial T}{\partial x}+v\frac{\partial T}{\partial y}=\alpha\left(\frac{\partial^2 T}{\partial x^2}+\frac{\partial^2 T}{\partial y^2}\right), \tag{4}$$

where $\rho=\rho_a[1-\beta(T-T_a)]$.

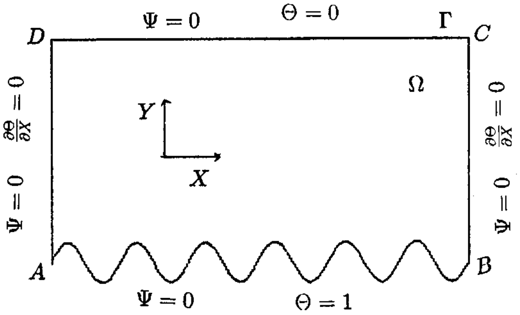

Figure 1. Porous enclosure with uniformly heated horizontal wavy wall.

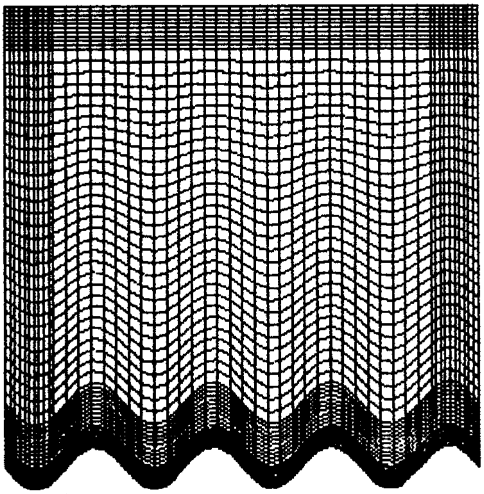

Figure 2. Five level graded finite element mesh.

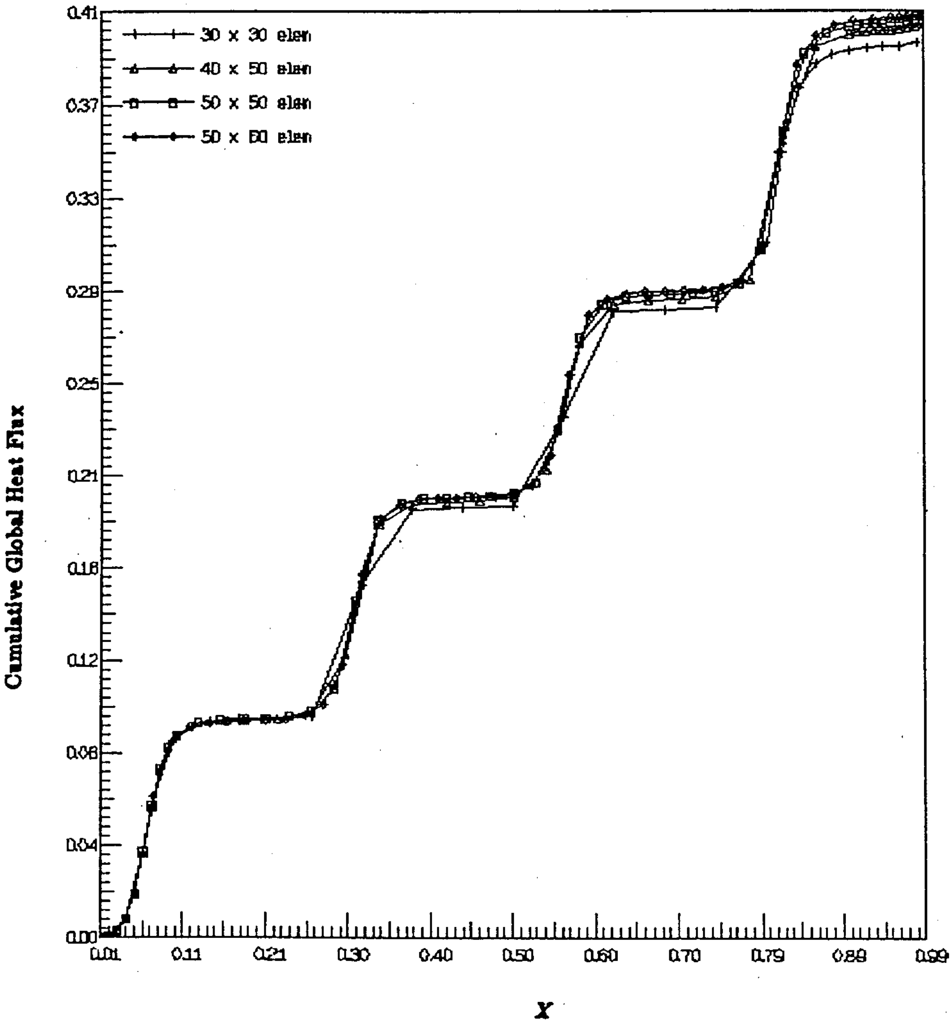

Figure 3. Mesh independency comparison for 30 × 30, 40 × 50, 50 × 50 and 50 × 60 quadratic serendipity elements.

Here x and y are the Cartesian co-ordinates, u and v are the velocity components in the x- and y-directions, respectively, T is the temperature, ρ is the density, p is the pressure, β is the coefficient of thermal expansion, μ is the viscosity of the fluid, K is the permeability constant, g is acceleration due to gravity and α is the thermal diffusivity constant.

Eliminating the pressure from the momentum equation and expressing the resulting momentum and energy equations in terms of the streamfunction and temperature variables by making use of the equations $u = -\partial\psi/\partial y$ and $v = \partial\psi/\partial x$, we get

$$\frac{\partial^2\psi}{\partial x^2} + \frac{\partial^2\psi}{\partial y^2} = \left(\frac{Kg\beta}{v}\right)\frac{\partial T}{\partial x}, \tag{5}$$

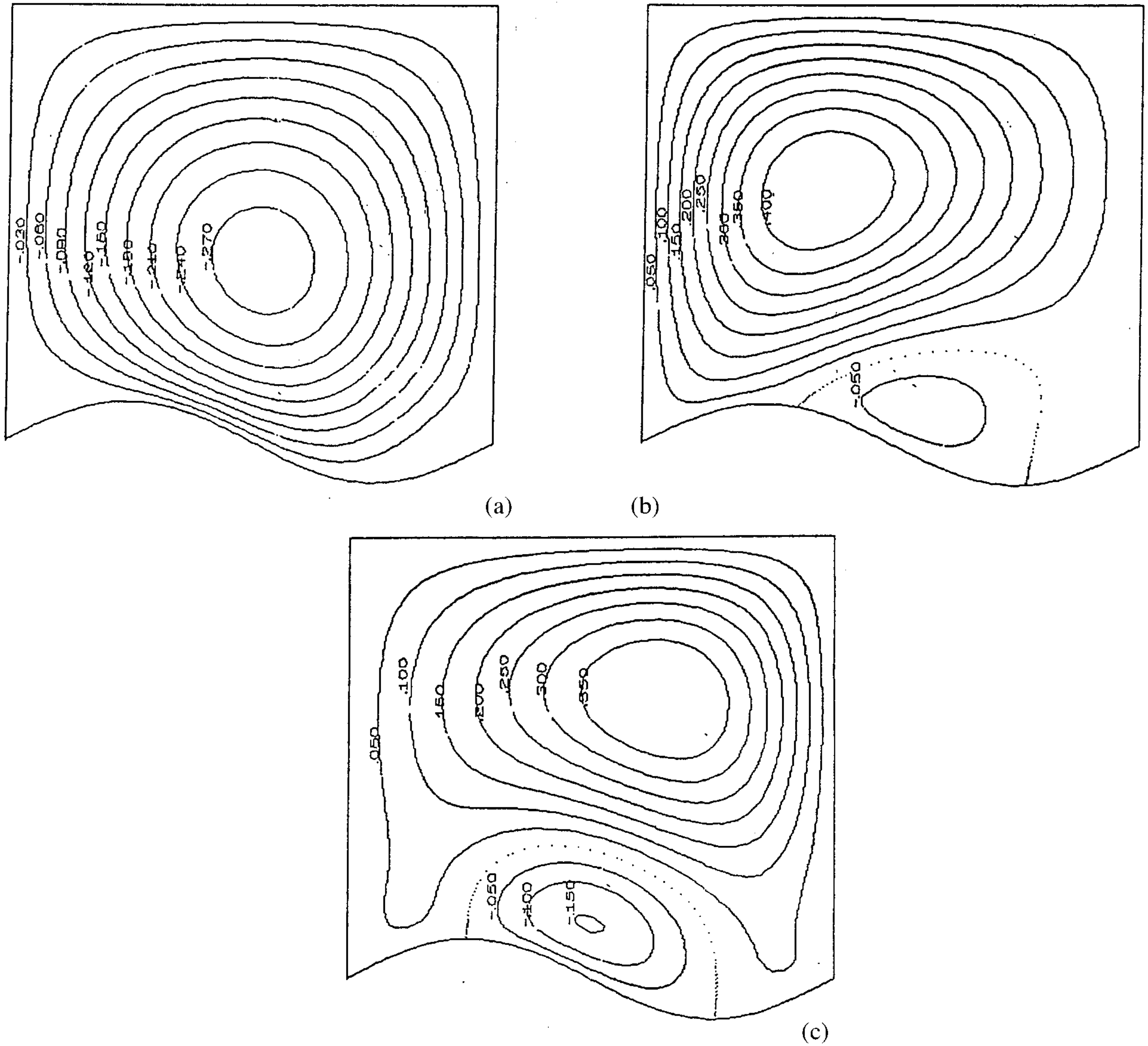

Figure 4. Streamlines for $N = 1$, $A = 1$, $a = 0.1$, $\phi = 0°$, and (a) $Ra = 25$, (b) $Ra = 50$, (c) $Ra = 75$.

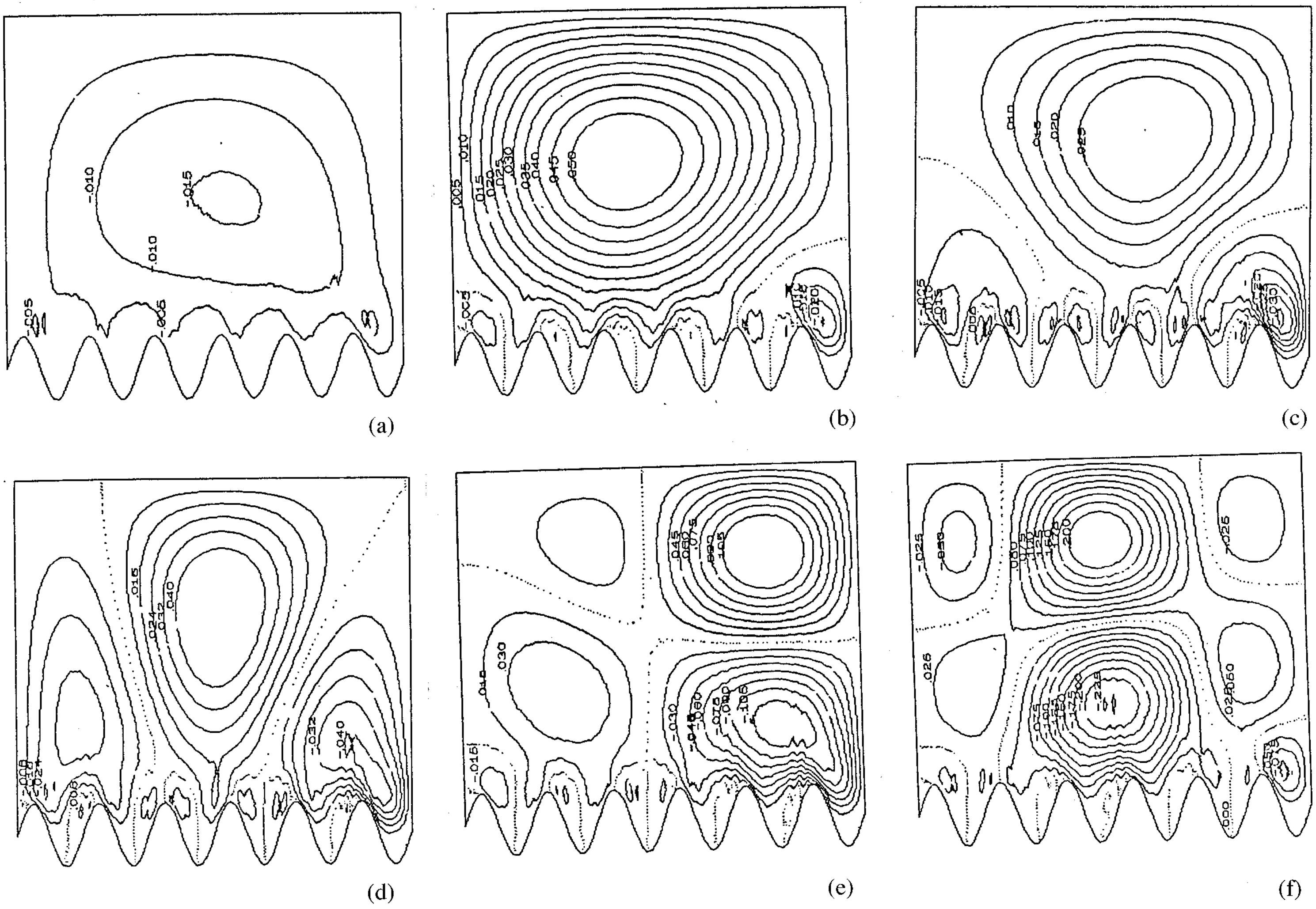

Figure 5 (*Continued*)

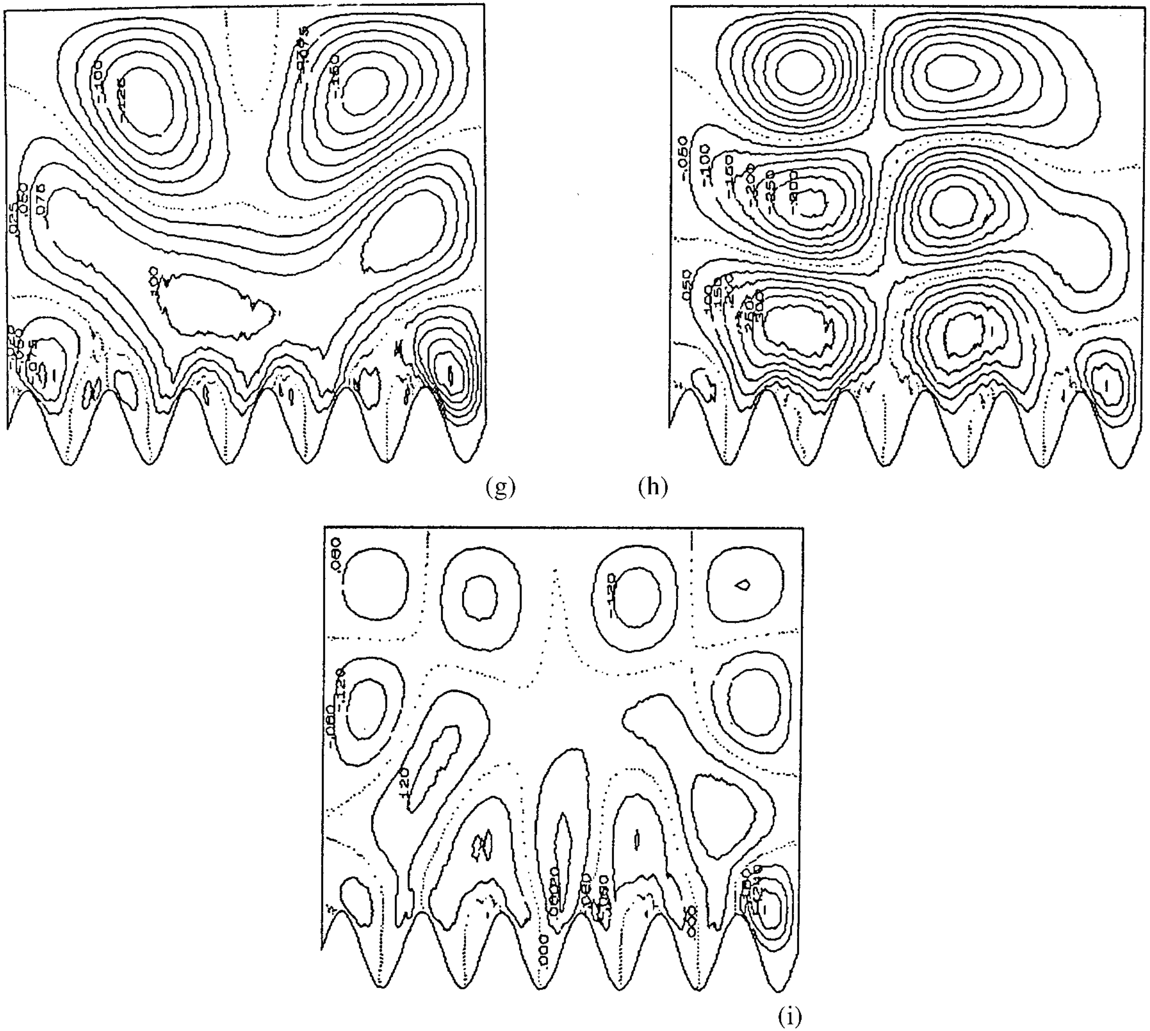

(g) (h)

(i)

Figure 5. Streamlines for $N = 6$, $A = 1$, $a = 0.1$, $\phi = 0°$, and (a) $Ra = 25$, (b) $Ra = 50$, (c) $Ra = 75$, (d) $Ra = 100$, (e) $Ra = 150$, (f) $Ra = 200$, (g) $Ra = 300$, (h) $Ra = 400$, (i) $Ra = 500$.

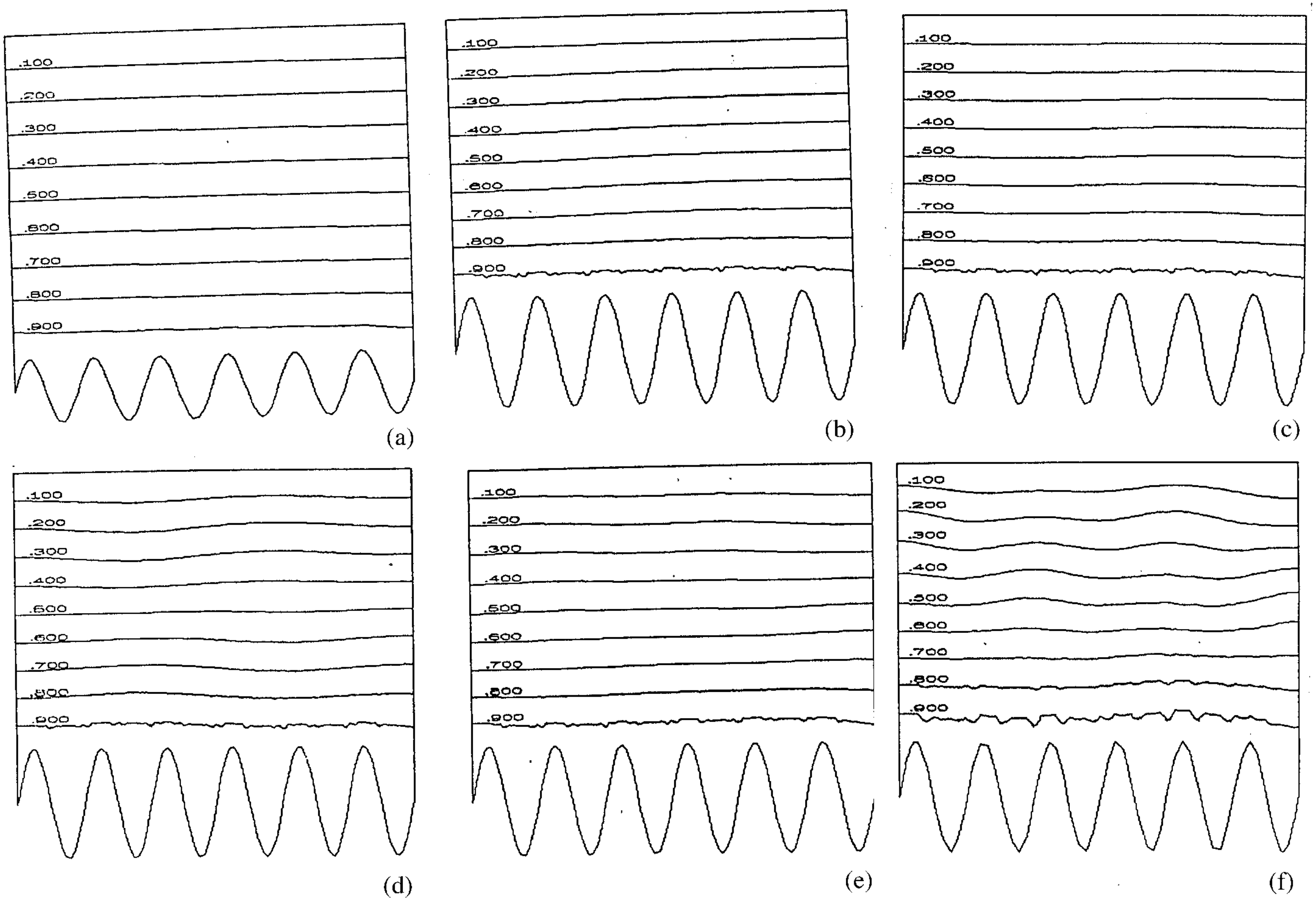

Figure 6. Isotherms for $N = 6$, $A = 1$, $a = 0.2$, $\phi = 0°$, and (a) $Ra = 50$, (b) $Ra = 100$, (c) $Ra = 200$, (d) $Ra = 300$, (e) $Ra = 400$.

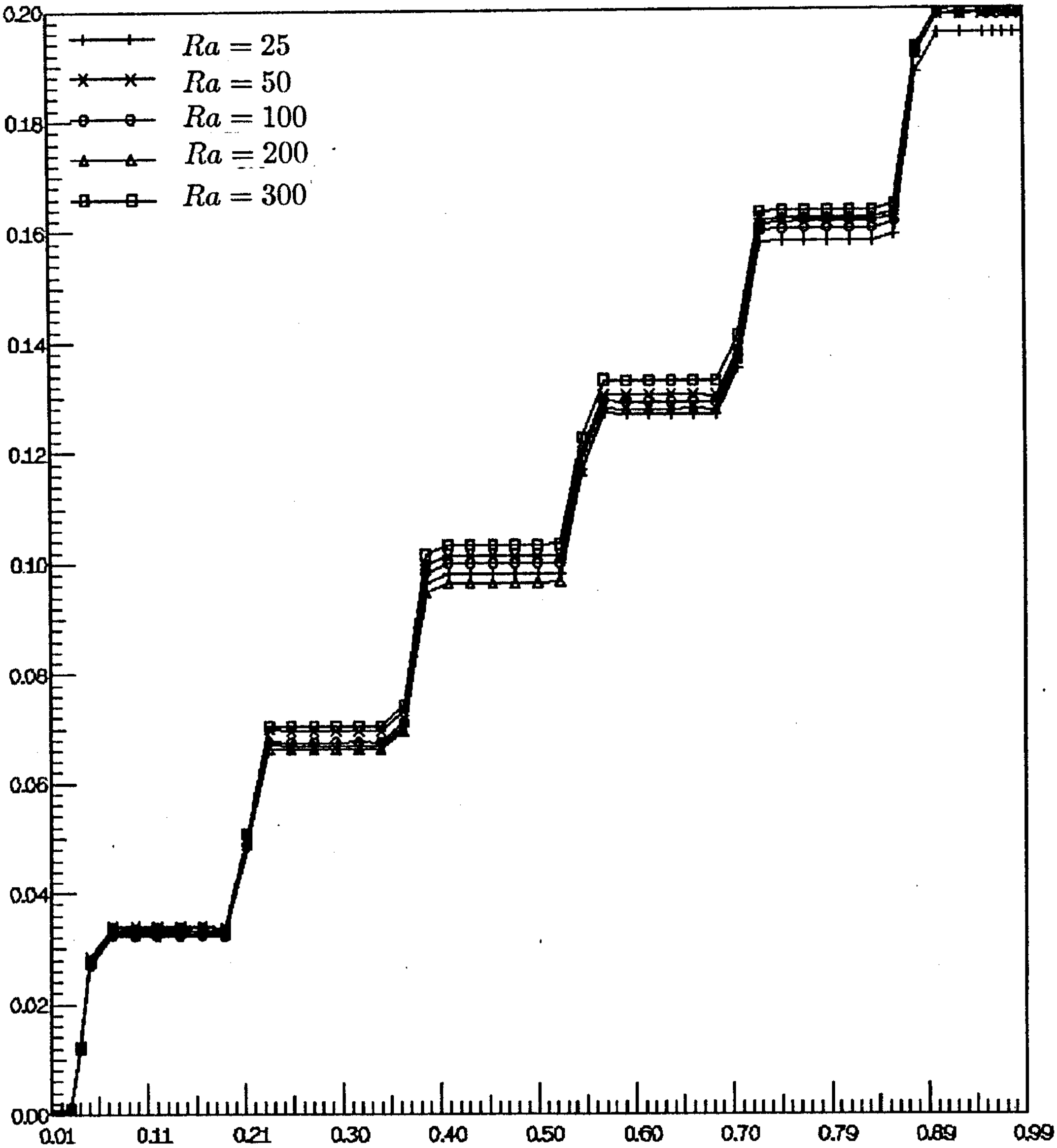

Figure 7. Cumulative heat flux vs. Ra for $N = 6$, $A = 1$, $a = 0.2$ and $\phi = 0°$.

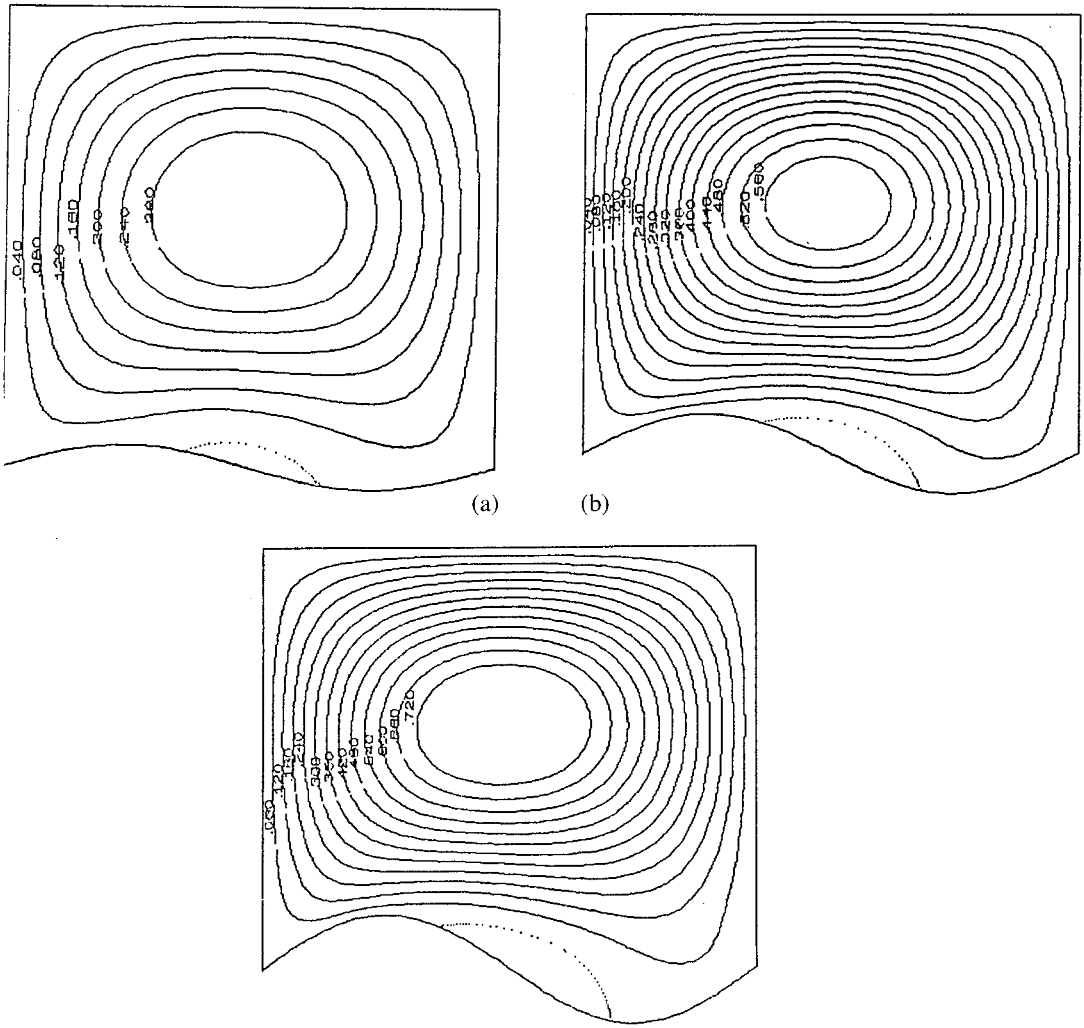

(a) (b)

(c)

Figure 8. Streamlines for $N=1$, $A=1$, $\phi=0°$, $Ra=50$ and (a) $a=0.05$, (b) $a=0.1$, (c) $a=0.15$.

$$\frac{\partial\psi}{\partial x}\frac{\partial T}{\partial y}-\frac{\partial\psi}{\partial y}\frac{\partial T}{\partial x}=\alpha\left[\frac{\partial^2 T}{\partial x^2}+\frac{\partial^2 T}{\partial y^2}\right]. \tag{6}$$

Now consider the following non-dimensional variables,

$$X=\frac{x}{L},\quad Y=\frac{y}{H},\quad \Psi=\frac{\psi}{\alpha},\quad \theta=\frac{T-T_{\mathrm{a}}}{T_{\mathrm{w}}-T_{\mathrm{a}}},\quad A=\frac{H}{L}\quad \text{and}\quad Ra=\frac{Kg\beta\theta_{\mathrm{w}}L}{\alpha\nu},$$

we get

$$A^2\frac{\partial^2\Psi}{\partial X^2}+\frac{\partial^2\Psi}{\partial Y^2}=-ARa\frac{\partial\theta}{\partial X}, \tag{7}$$

$$\frac{\partial\Psi}{\partial X}\frac{\partial\theta}{\partial Y}-\frac{\partial\Psi}{\partial Y}\frac{\partial\theta}{\partial X}=\frac{\partial^2\theta}{\partial X^2}+\frac{1}{A^2}\frac{\partial^2\theta}{\partial Y^2}, \tag{8}$$

and the transformed boundary conditions will be

$$\left.\begin{array}{r}\Psi=0 \text{ on all boundaries}\\ \theta=1 \text{ on } Y=a\sin(N\pi X-\phi)\\ \theta=0 \text{ on } Y=1\\ \dfrac{\partial\theta}{\partial X}=0 \text{ on } X=0 \text{ and } X=1\end{array}\right\}. \tag{9}$$

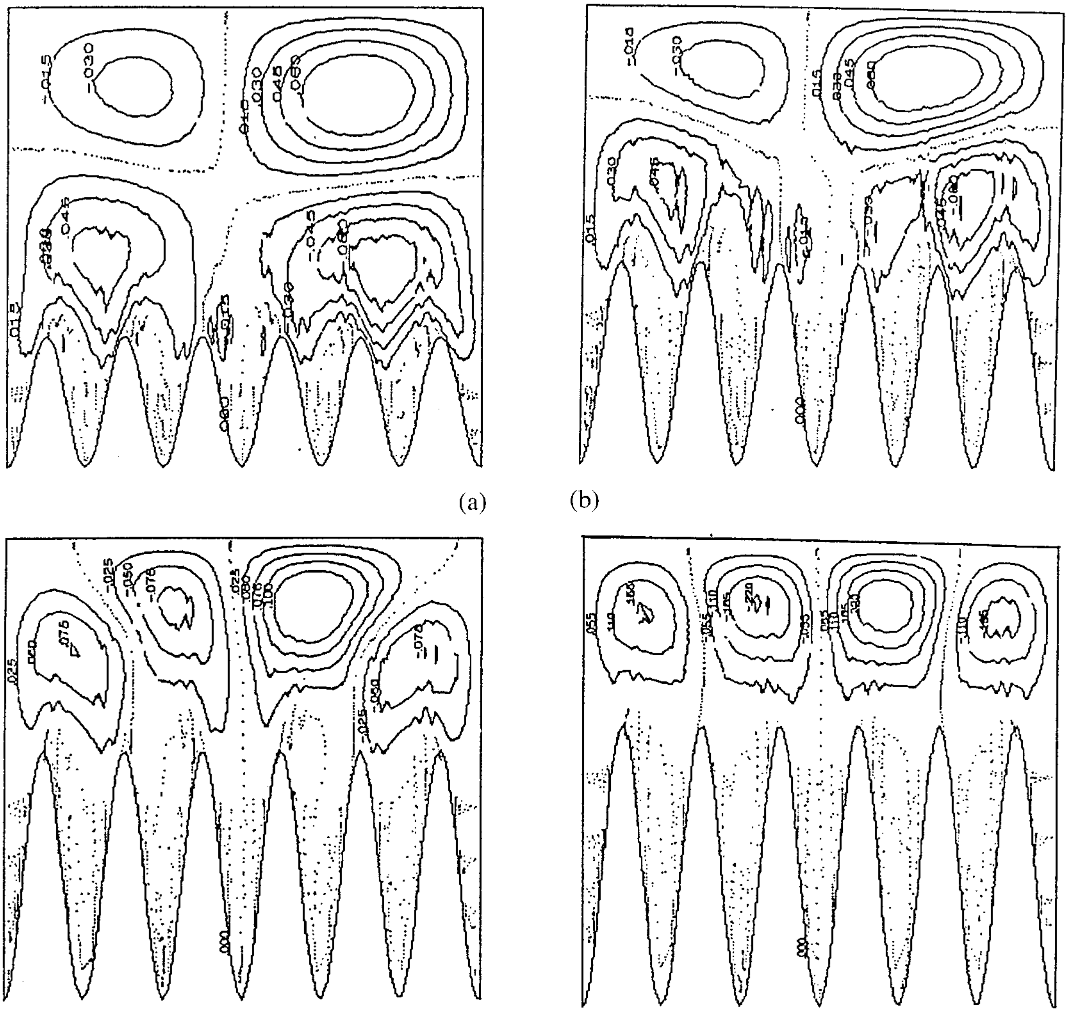
(a) (b) (c) (d)

Figure 9. Streamlines for $N=6$, $A=1$, $Ra=150$ and (a) $a=0.2$, (b) $a=0.4$, (c) $a=0.6$, (d) $a=0.8$.

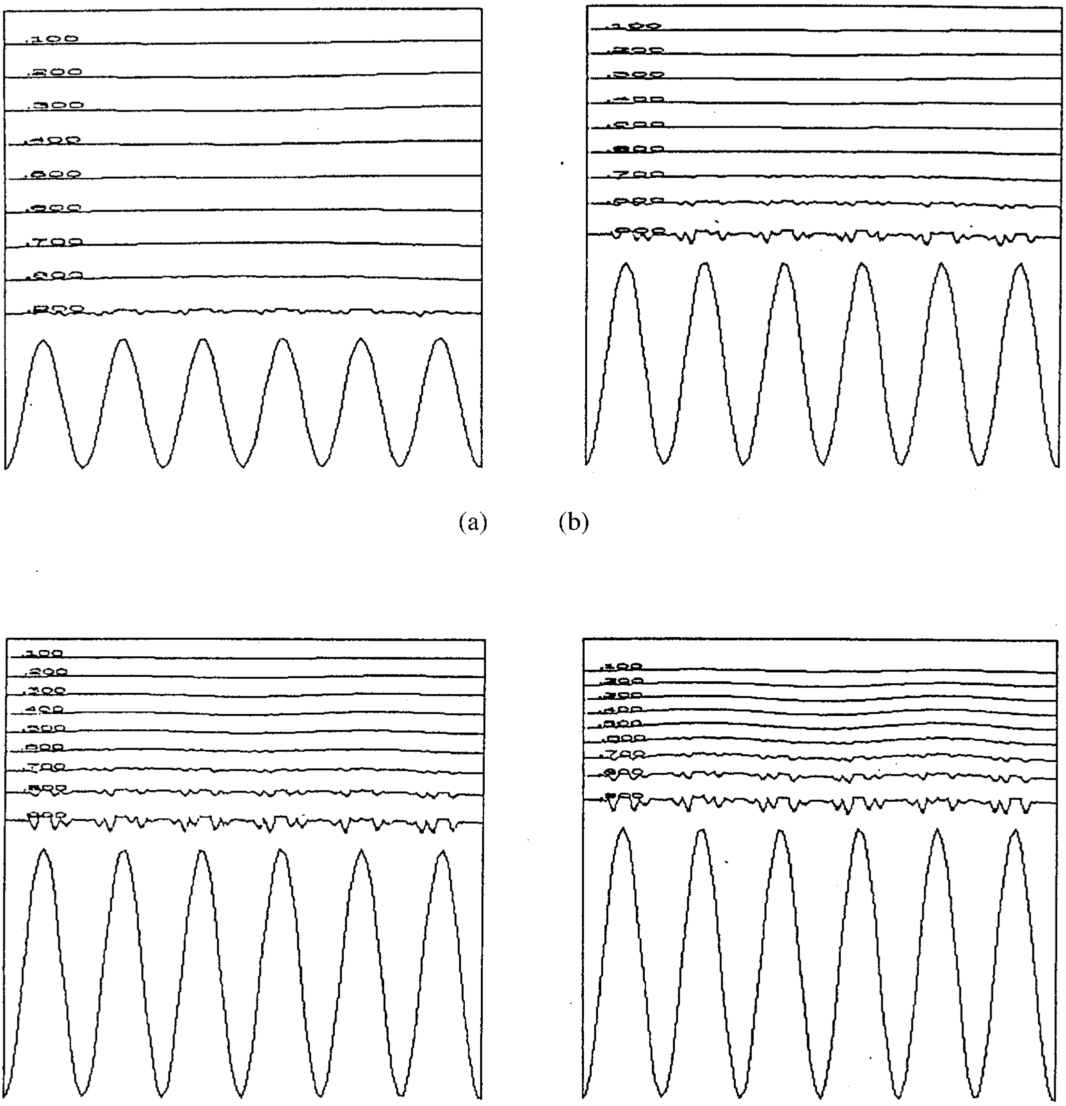

(a) (b)

(c) (d)

Figure 10. Isotherms for $N = 6$, $A = 1$, $Ra = 150$ and (a) $a = 0.2$, (b) $a = 0.4$, (c) $a = 0.6$, (d) $a = 0.8$.

Here X and Y are the dimensionless Cartesian co-ordinates, H is the length of the side walls of the cavity, L is the length of the bottom wall, A is the aspect ratio, ψ and Ψ are dimensional and dimensionless streamfunctions, respectively, T is the temperature, T_w. is the wall temperature, T_a is the reference temperature, θ is the dimensionless temperature and N is the number of waves considered per unit length of the wall.

The resulting partial differential equations (7) and (8), along with the hydrodynamic and thermal boundary conditions equation (9), are solved numerically using Bubnov–Galerkin's weighted residual finite element technique.

3. NUMERICAL ANALYSIS

To precisely accommodate the geometrical non-linearity owing to the wavy nature of the wall, the domain $A\ B\ C\ D$ (Figure 1) has been discretized using isoparametric quadratic serendipity elements with finer elements near the boundaries.

The Galerkin weighted residual form of the momentum equation and the energy equation are

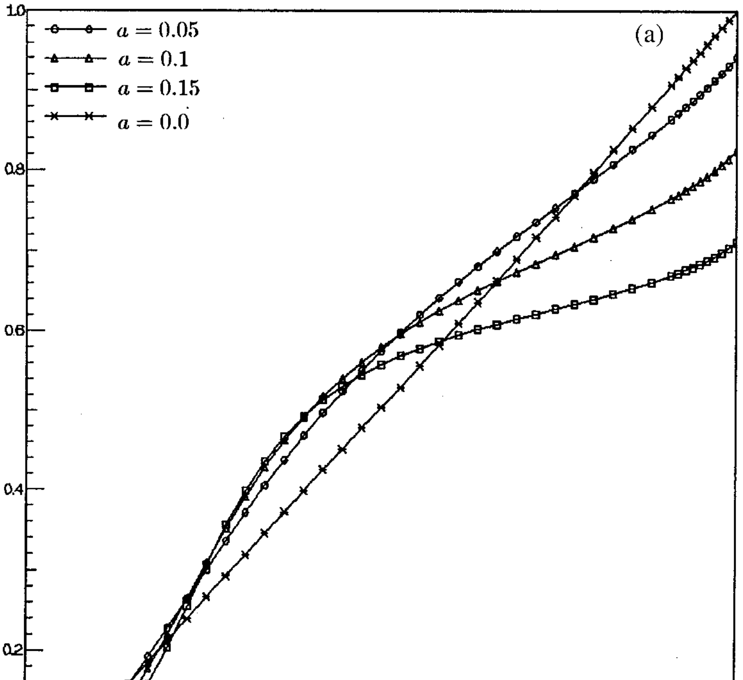

Figure 11. (a) Cumulative heat flux vs. a for $N = 1$, $A = 1$, $Ra = 50$, and $\phi = 0°$. (b) Cumulative heat flux vs. a for $N = 6$, $A = 1$, $Ra = 150$, $\phi = 90°$.

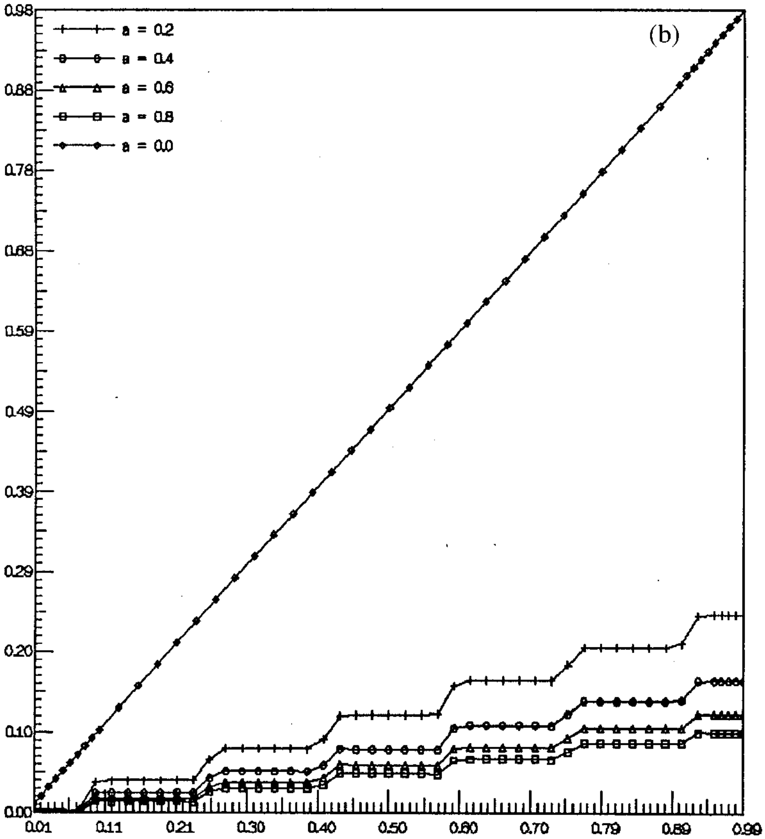

Figure 11 (*Continued*)

$$\int_{\Omega}\left(A^2\frac{\partial^2\Psi}{\partial X^2}+\frac{\partial^2\Psi}{\partial Y^2}+ARa\frac{\partial\theta}{\partial X}\right)W_l\,\mathrm{d}\Omega=0, \tag{10}$$

$$\int_{\Omega}\left[\frac{\partial^2\theta}{\partial X^2}+\frac{1}{A^2}\frac{\partial^2\theta}{\partial Y^2}+\left(\frac{\partial\Psi}{\partial Y}\frac{\partial\theta}{\partial X}-\frac{\partial\Psi}{\partial X}\frac{\partial\theta}{\partial Y}\right)\right]W_l\,\mathrm{d}\Omega=0. \tag{11}$$

Introducing the following discretization of the domain $(\Omega\cup\Gamma)$ and the element level discretized representation for the streamfunction and temperature distribution

$$\Omega=\bigcup_e\Omega^e$$

$$\Psi=\sum_{i=1}^{i=8}\Psi_i^eN_i^e,\quad \theta=\sum_{i=1}^{i=8}\theta_i^eN_i^e\quad\text{and}\quad W_l=N_l^e,$$

into Equations (10) and (11), we obtain the following elemental matrix over a typical element e as

$$\mathbf{M}^e\cdot r^e=f^e, \tag{12}$$

where

$$\mathbf{M}^e=\begin{bmatrix}A_{lk}^e & B_{lk}^e\\ C_{lki}^e & D_{lk}^e\end{bmatrix},$$

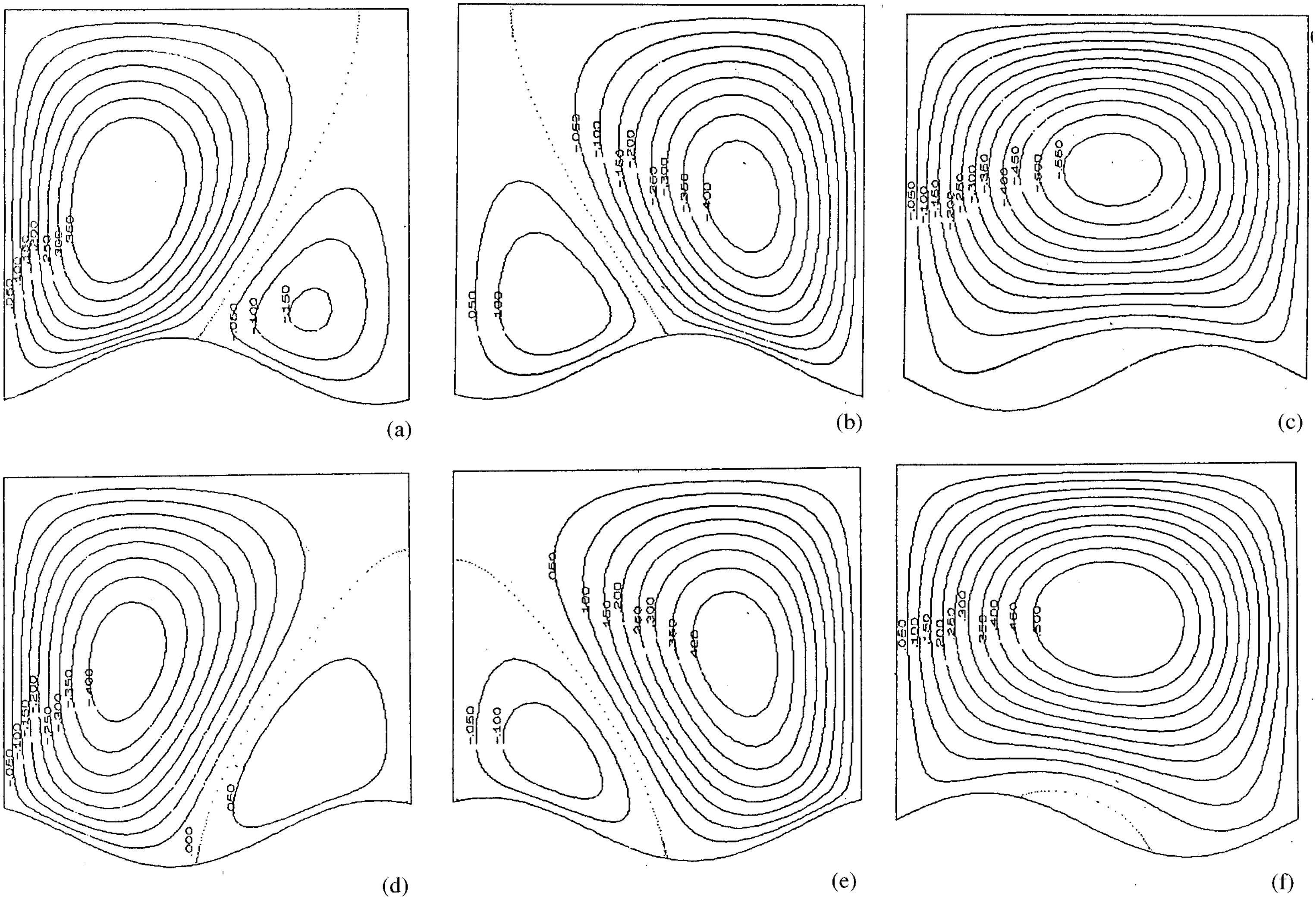

Figure 12. Streamlines for $N = 1$, $A = 1$, $Ra = 50$, $a = 0.1$ and (a) $\phi = 60°$, (b) $\phi = 120°$, (c) $\phi = 180°$, (d) $\phi = 240°$, (e) $\phi = 300°$, (f) $\phi = 350°$.

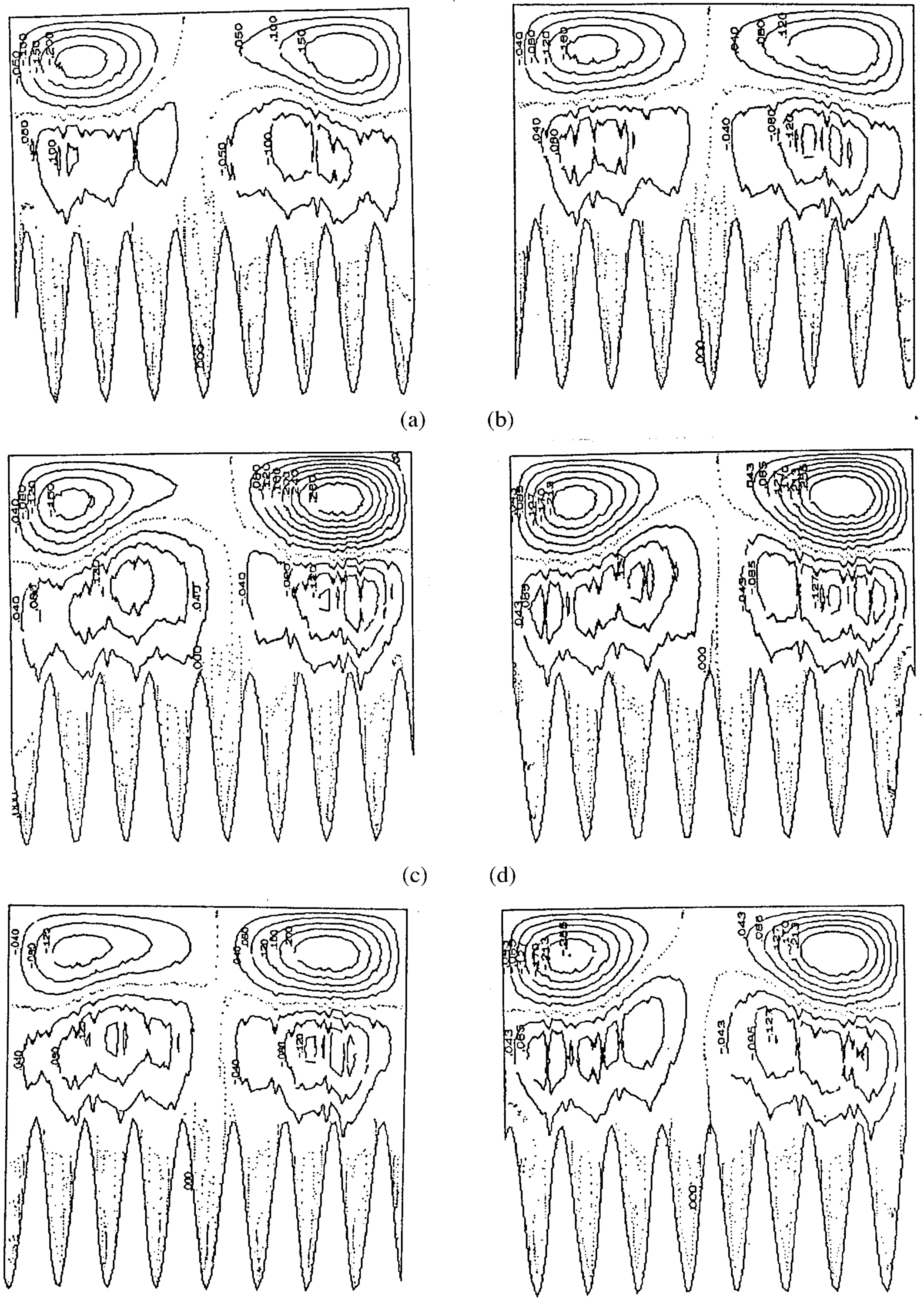

Figure 13. Streamlines for $N = 8$, $A = 1$, $Ra = 200$, $a = 0.4$ and (a) $\phi = 0°$, (b) $\phi = 60°$, (c) $\phi = 120°$, (d) $\phi = 180°$, (e) $\phi = 240°$, (f) $\phi = 300°$.

and r^e is the column vector of unknown nodal parameters

$$r^e = [\Psi^e_k \quad \theta^e_k]^T,$$

and f^e is the known vector which is given by

$$f^e = [f^1_k \quad f^2_k]^2,$$

where

$$A^e_{lk} = -\int_{\Omega^e} \left(A^2 \frac{\partial N^e_l}{\partial X} \frac{\partial N^e_k}{\partial X} + \frac{\partial N^e_l}{\partial Y} \frac{\partial N^e_k}{\partial Y} \right) \mathrm{d}\Omega^e, \tag{13}$$

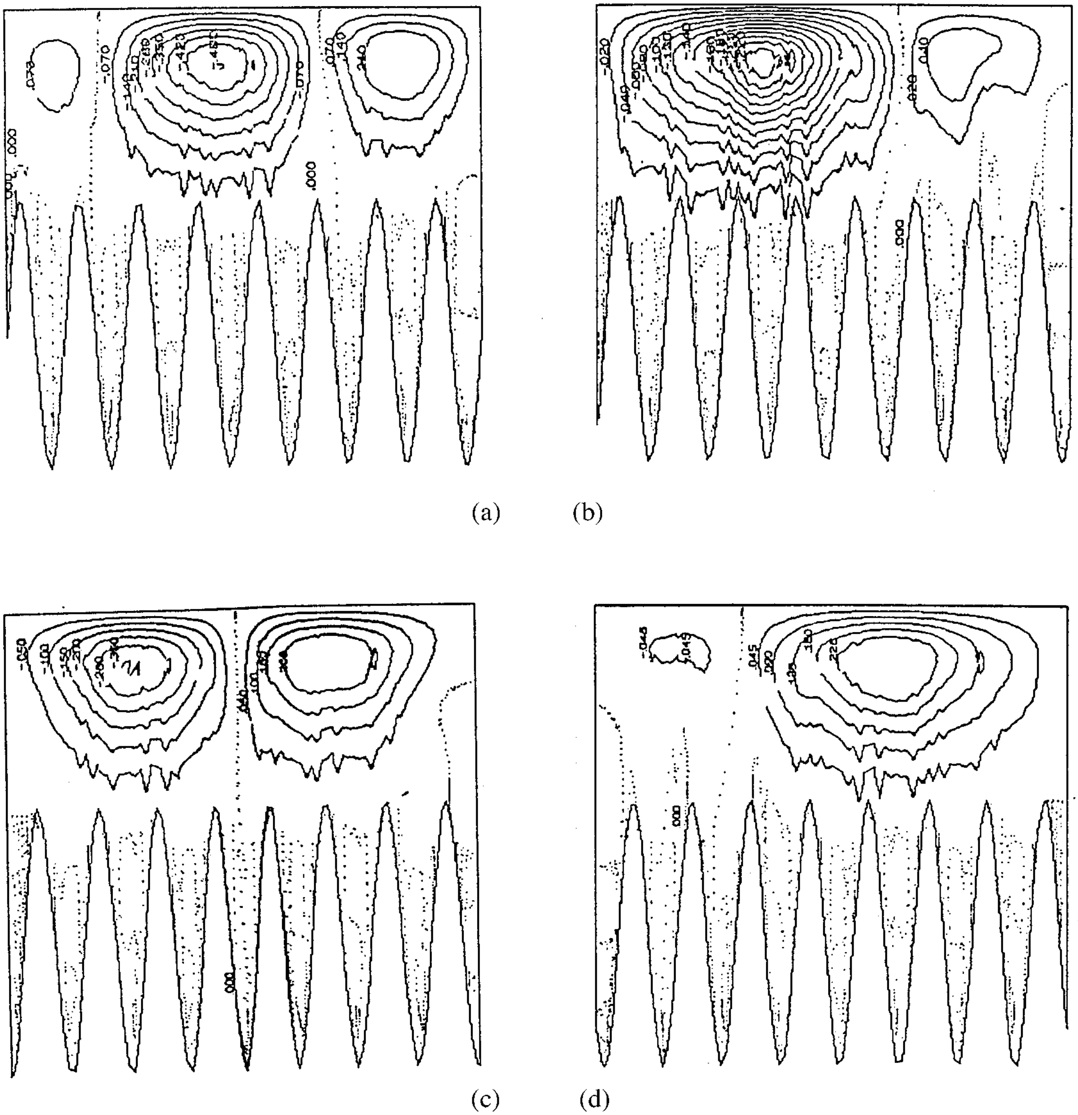

(a) (b)

(c) (d)

Figure 14. Streamlines for $N = 8$, $A = 1$, $Ra = 100$, $a = 0.7$ and (a) $\phi = 0°$, (b) $\phi = 45°$, (c) $\phi = 90°$, (d) $\phi = 135°$, (e) $\phi = 180°$, (f) $\phi = 225°$, (g) $\phi = 270°$, (h) $\phi = 315°$.

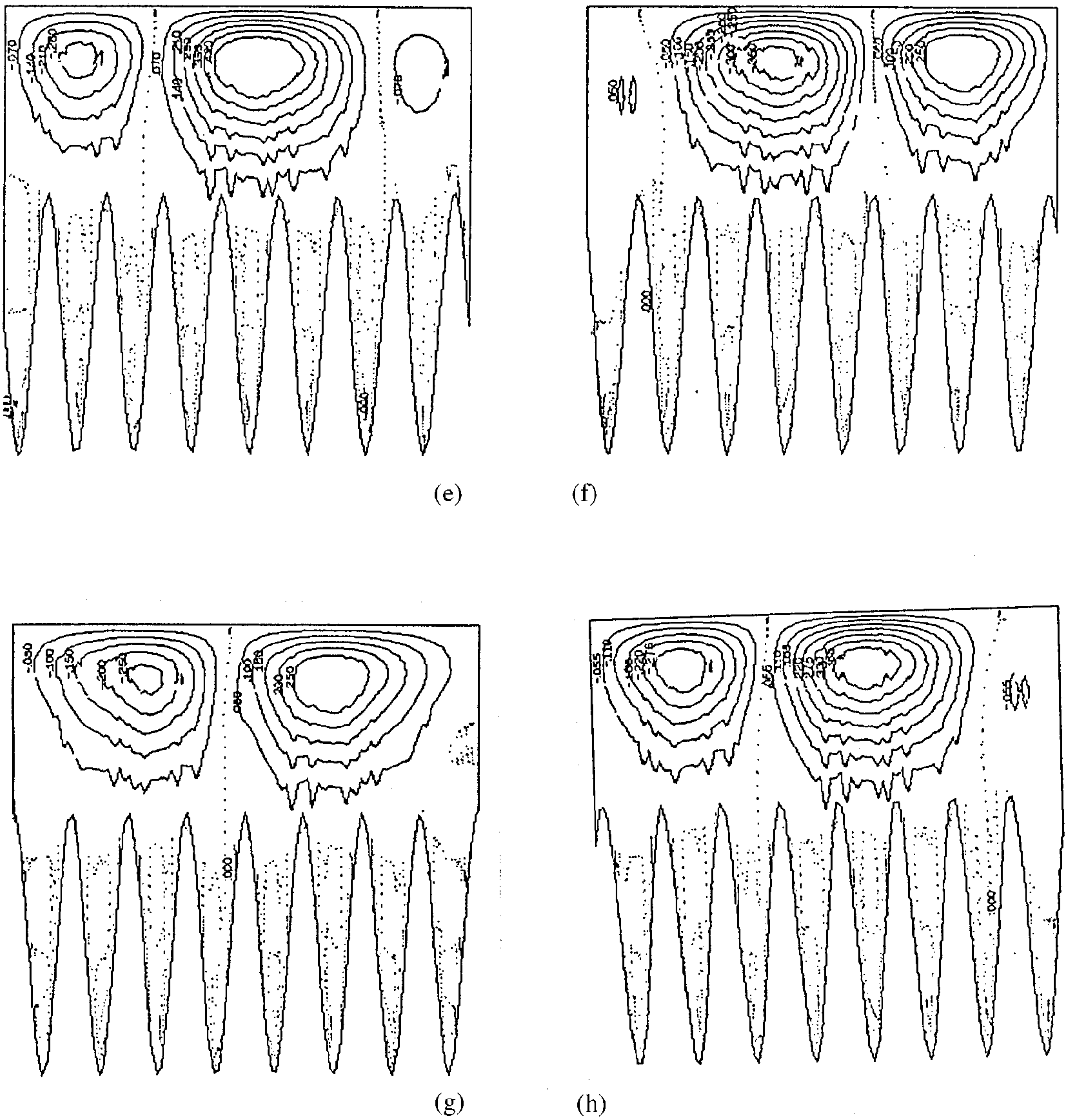

(e) (f)

(g) (h)

Figure 14 (*Continued*)

$$B^e_{lk} = Ra \int_{\Omega^e} A N^e_l \frac{\partial N^e_k}{\partial X}\, \mathrm{d}\Omega^e, \tag{14}$$

$$C^e_{lki} = \int_{\Omega^e} \sum_{i=1}^{i=8} \left(\frac{\partial N^e_k}{\partial X} \frac{\partial N^e_i}{\partial Y} N^e_l - \frac{\partial N^e_k}{\partial Y} \frac{\partial N^e_i}{\partial X} N^e_l \right) \mathrm{d}\Omega^e, \tag{15}$$

$$D^e_{lk} = -\int_{\Omega^e} \left(\frac{\partial N^e_l}{\partial X} \frac{\partial N^e_k}{\partial X} + \frac{1}{A^2} \frac{\partial N^e_l}{\partial Y} \frac{\partial N^e_k}{\partial Y} \right) \mathrm{d}\Omega^e. \tag{16}$$

In the view of the finite element assembly procedure and the prescribed essential and natural boundary conditions, without any loss of generality, the components of f^e can be written as

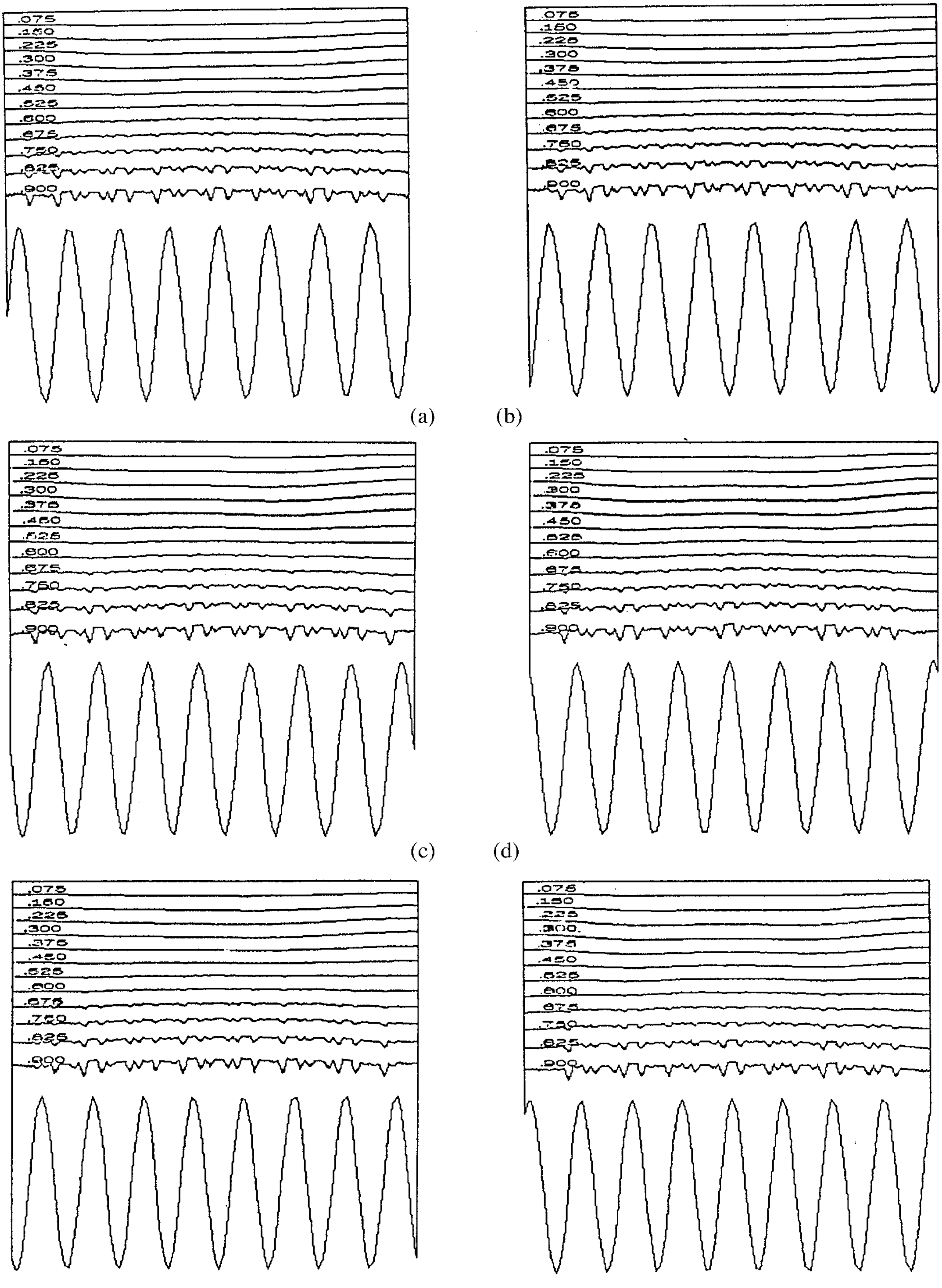

Figure 15. Isotherms for $N = 8$, $A = 1$, $Ra = 200$, $a = 0.4$ and (a) $\phi = 0$, (b) $\phi = 60°$, (c) $\phi = 120°$, (d) $\phi = 180°$, (e) $\phi = 240°$, (f) $\phi = 300°$.

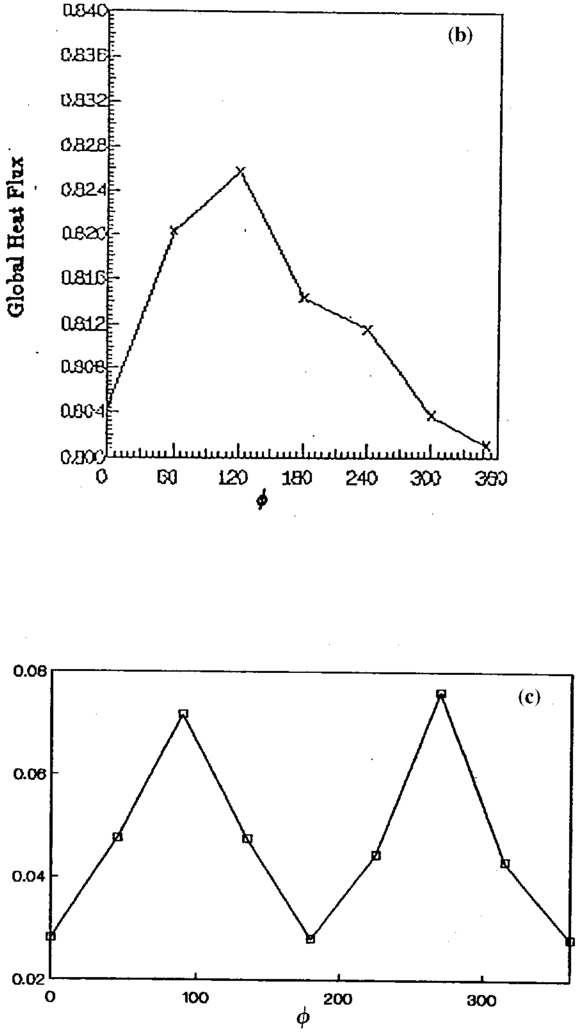

Figure 16 (*Continued*)

Numerical simulations have been carried out on a 50 × 60 graded finite element mesh as shown in Figure 2. Newton Raphson's method, in conjunction with the Frontal solver has been used to solve the system of algebraic equations resulting from the assembly of the elemental equations. The results have been obtained to an accuracy of 5×10^{-4}. To ensure the grid independency of the results, the numerical experiments were carried out on five different mesh systems consisting of 30 × 30, 40 × 40, 40 × 50, 50 × 50 and 50 × 60 elements and the 50 × 60 mesh has been chosen for accurate computations. The value of cumulative global heat flux has been plotted for this comparison, as shown in the Figure 3. It clearly shows that the change in global heat flux becomes negligible as it moves from the 30 × 30 mesh system to the 50 × 60 mesh system. Further, the results obtained on the 50 × 50 and 50 × 60 mesh systems look identical.

$$f_l^1 = 0, \tag{17}$$

$$f_l^2 = -\int_{\Gamma^{2+4}\cap\Gamma^e} M_f N_l \overline{\frac{\partial\theta}{\partial n}}\, \mathrm{d}\Gamma^e, \tag{18}$$

where the expression under the overbar denotes the prescribed normal heat flux and M_f is defined as

$$M_f = 1 \text{ if } \bar{n} \text{ is parallel to the } X\text{-axis and } M_f = \frac{1}{A^2} \text{ if } \bar{n} \text{ is parallel to the } Y\text{-axis.}$$

It is of interest to study the net effect of the geometrical parameters on the free convective heat transfer in a porous enclosure. For this purpose, the cumulative global heat flux has been computed from the formula

$$Q_X = \int_0^X (n \cdot \nabla T)\, \frac{\mathrm{d}s(\xi)}{\mathrm{d}\xi}\, \mathrm{d}\xi, \tag{19}$$

where n is the outward drawn normal to the wavy surface and $s(\xi)$ is the arc length along the surface with the arc length variable, ξ. The global heat flux can be obtained from the above expression by taking $X = 1$ in the integral limit.

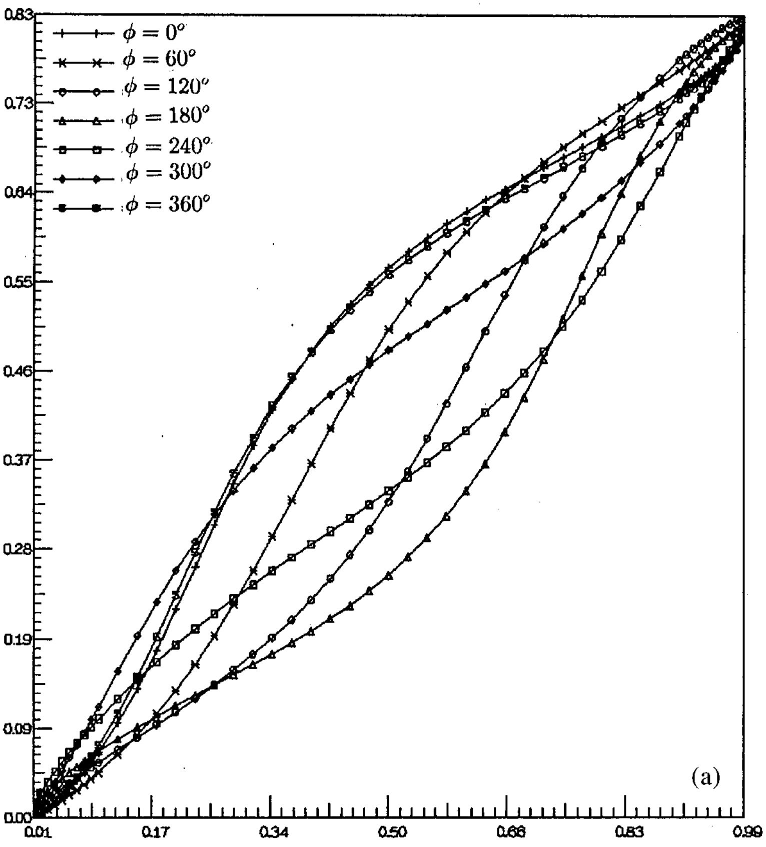

Figure 16. (a) Cumulative heat flux vs. ϕ for $N = 1$, $A = 1$, $a = 0.1$ and $Ra = 50$. (b) Single wave case: global heat flux vs. phase. (c) Multiple wave case: global heat flux vs. phase.

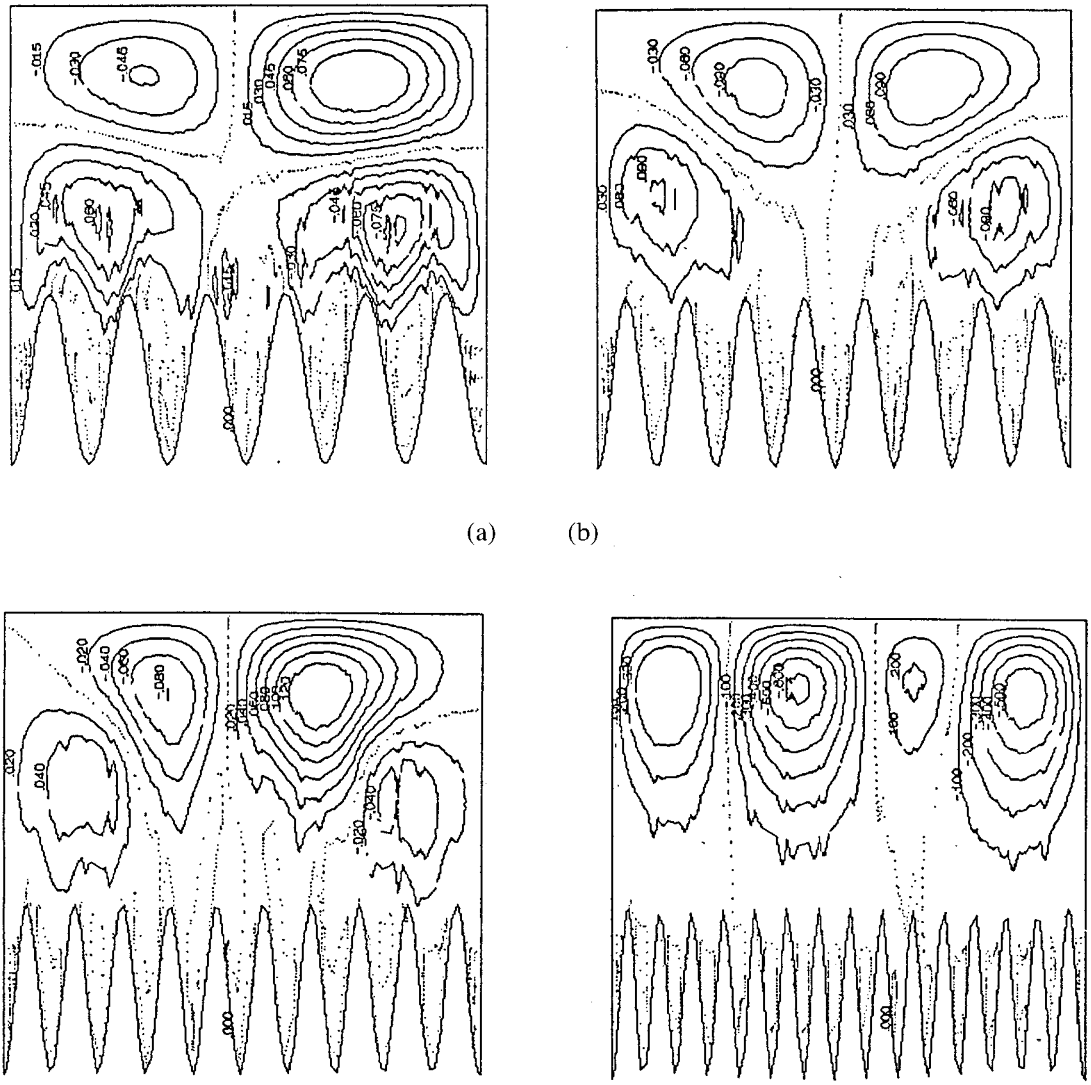

(a) (b)

(c) (d)

Figure 17. Streamlines for $Ra = 150$, $a = 0.3$, $A = 1$, $\phi = 90°$, and (a) $N = 6$, (b) $N = 8$, (c) $N = 10$, (d) $N = 15$.

4. RESULTS AND DISCUSSION

The parameters which are found to influence the flow and heat transfer in a porous enclosure are the modified Rayleigh number, Ra, based on the length of the wavy wall, the amplitude (a) and the phase (ϕ) of the wave, the number (N) of the waves per unit length of the wavy wall and aspect ratio (A) of the porous enclosure.

To begin with, the flow and heat transfer process have been analyzed in a porous enclosure with a single wave ($N = 1$) of amplitude $a = 0.1$, with phase $\phi = 0°$ and aspect ratio $A = 1$ and for $Ra = 25$, 50, 75. For $Ra = 50$, a flow separation and reattachment on the wavy wall is observed. This is seen from the streamlines in Figure 4. The flow separation and reattachment can be attributed to the change in pressure gradient, owing to the non-linear geometry of the bottom wall. With increasing *Ra*, the separation and reattachment points move closer to the leading and trailing edges, respectively, and also the size of the secondary circulation zone increases. In the multiple wave case, the flow has been analyzed for $Ra = 25$ to $Ra = 500$ with $a = 0.1$, $\phi = 0°$, $A = 1$ and $N = 6$. Streamlines corresponding to this study are given in Figure 5(a)–(h). At small values of *Ra*, a primary circulation zone with wavy streamlines close to the horizontal isothermal undulated wall and small secondary circulation zones in the concavity of the waves are noticed. With the increase in *Ra*, several prominent circulation zones appear in the core of the domain. As *Ra* increases, unicellular flow transforms to a multicellular flow, with the flow in adjacent cells in the opposite direction. Streamline profiles suggest that the

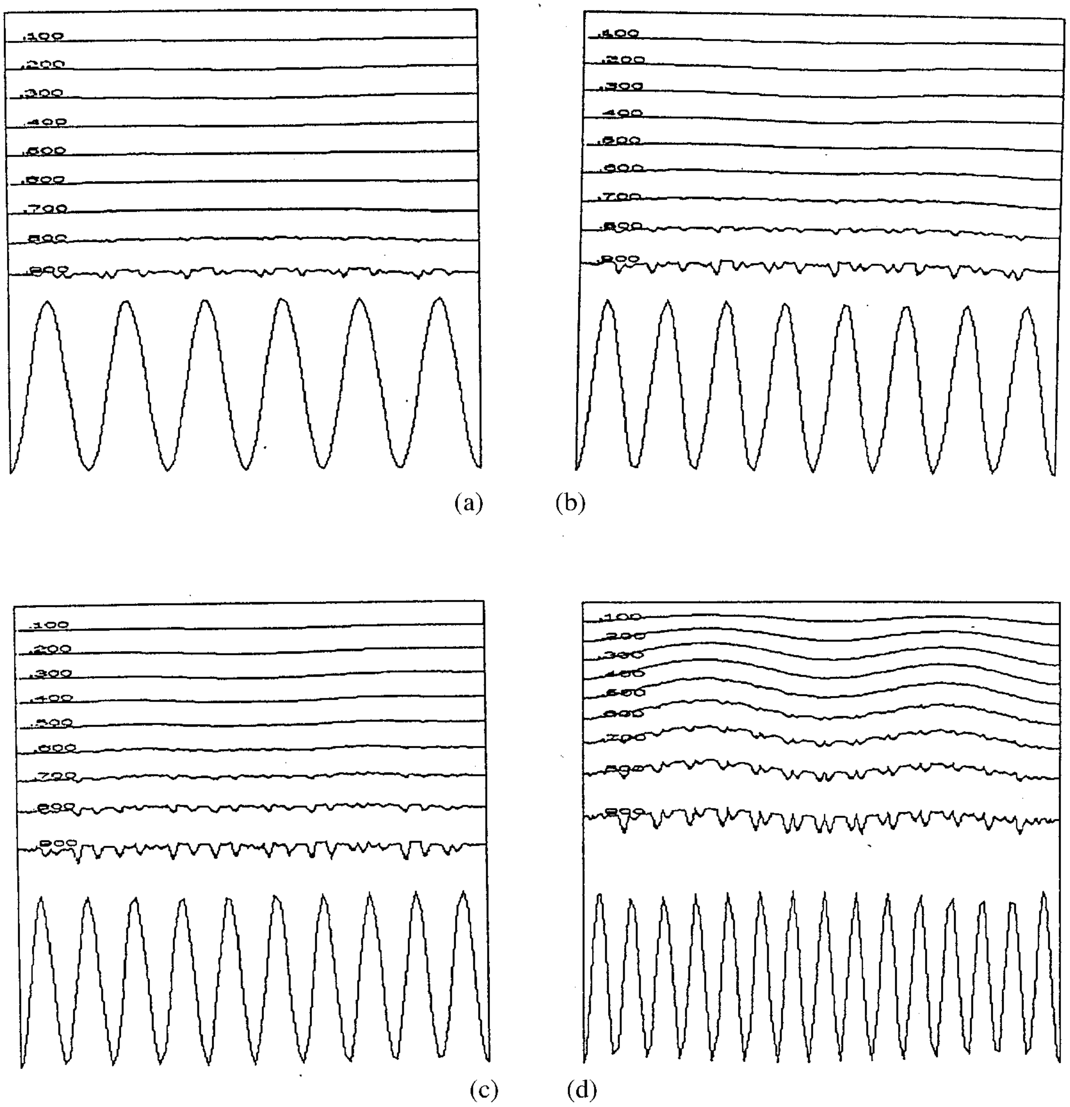

Figure 18. Isotherms for $Ra = 150$, $a = 0.3$, $A = 1$, $\phi = 90°$, and (a) $N = 6$, (b) $N = 8$, (c) $N = 10$, (d) $N = 15$.

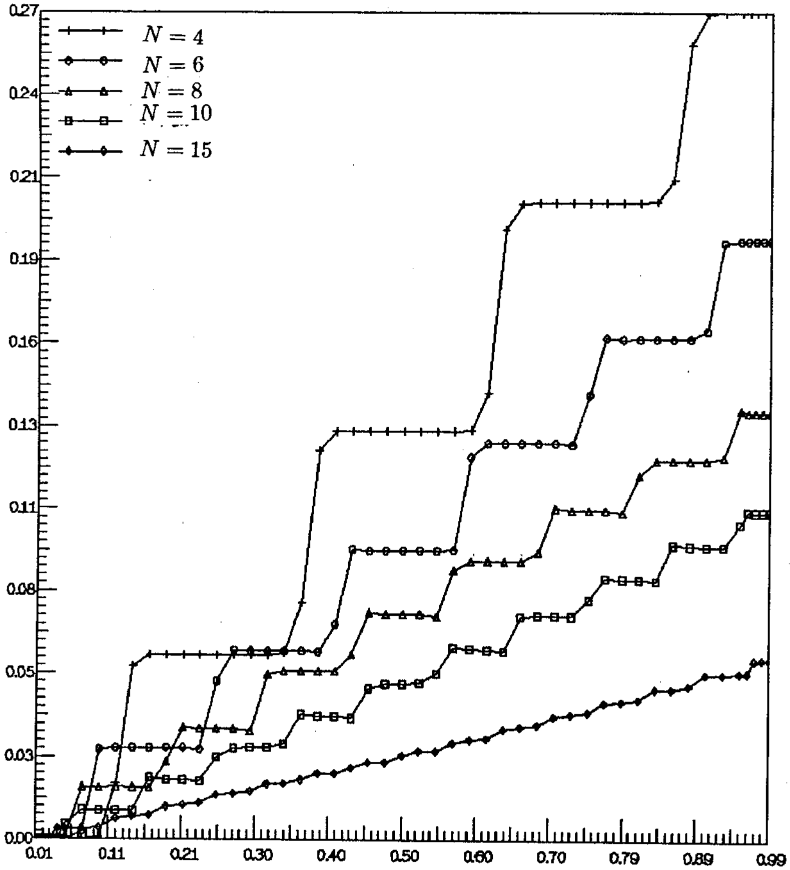

Figure 19. Cumulative heat flux vs. N for $Ra = 150$, $a = 0.3$, $A = 1$, $\phi = 90°$.

secondary flow regions developing on the wavy wall increase with increasing *Ra*, slowly spread into the core of the domain and later get detached and move away from the wavy wall. This supports the convection-favouring nature of increasing *Ra*. The transformation of the unicellular pattern to multicellular pattern may be attributed to the enhancement of buoyancy force brought in by increasing *Ra*. As secondary recirculation zones are known to hinder the heat transfer process, it would be essential to analyze the convection process. In Figure 6(a)–(e), isotherms for $Ra = 50$ to $Ra = 400$ are presented. Owing to the wavy nature of the bottom surface, isotherms close to the bottom wall are wavy in nature and this percolates into the rest of the domain with increasing *Ra*. Better insight into the convection process can be obtained from global heat flux plots. So, in Figure 7, cumulative heat flux is plotted against *Ra*. End values of the cumulative heat flux plots will give us the global heat flux. From these plots we find that there are only marginal changes in the global heat flux into the domain with increasing *Ra*. Lack of clear trends in the global heat flux can be attributed to the presence of two competing factors, one favoring and the other opposing the convection process. The favoring factor is buoyancy force, which is enhanced by increasing *Ra* and the opposing factor is a secondary recirculation zone, whose number and size are increased by increasing *Ra*. The net effect of these two factors bring about only a marginal change in the global heat flux.

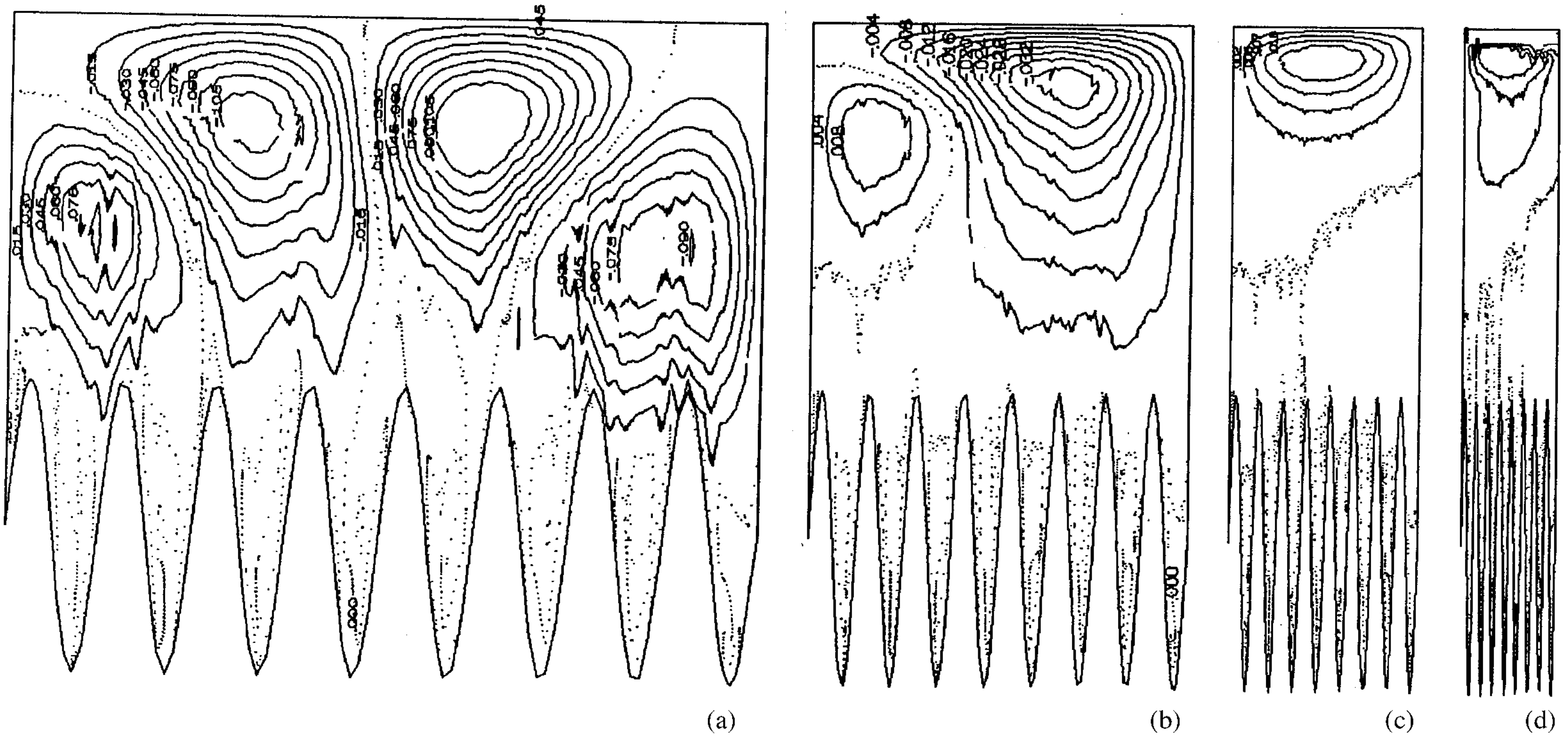

Figure 20. Streamlines for $Ra = 150$, $\phi = 0°$, $a = 0.4$, $N = 8$, and (a) $A = 1$, (b) $A = 2$, (c) $A = 4$, (d) $A = 8$.

The effect of varying amplitude was initially studied for the single wave case at $Ra = 50$, $\phi = 0°$, $A = 1$, $N = 1$ and $a = 0.05$, 0.1, 0.15 and the streamlines are presented in Figure 8(a)–(c). The secondary circulation region seen on the wavy wall grows in dimensions of increasing amplitude. The studies in the multiple wave case has been carried out for $a = 0.2$, 0.4, 0.6, 0.8; $Ra = 150$; $\phi = 90$; $A = 1$ and $N = 6$. The streamlines corresponding to this study are presented in Figure 9(a)–(d). At all amplitudes, owing to the Ra at which the simulation is carried out, a multicellular flow pattern is observed. At small amplitudes, the flow separates and reattaches on the adjacent walls of the domain in an anticlockwise direction and thereby gives rise to a row–column pattern of secondary circulation zones. As amplitude increases, the number of circulation zones remain the same but the flow separates and reattaches on the bottom surface and thus leads to the formation of circulation zones in a simple row pattern. It is also observed that at small amplitudes, the flow in the right half of the domain is more intense and at higher amplitudes, the flow in the central circulation region is more intense. Isotherms corresponding to this case are presented in Figure 10(a)–(d). The isotherms close to the wavy wall are wavy and this feature extends deep into the domain with increasing values of amplitude. The cumulative heat flux plots, corresponding to single and multiple wave cases are presented in Figure 11(a) and (b). They depict that the total heat flux into the system decreases with increasing values of amplitude. Here the heat flux from a flat surface is also

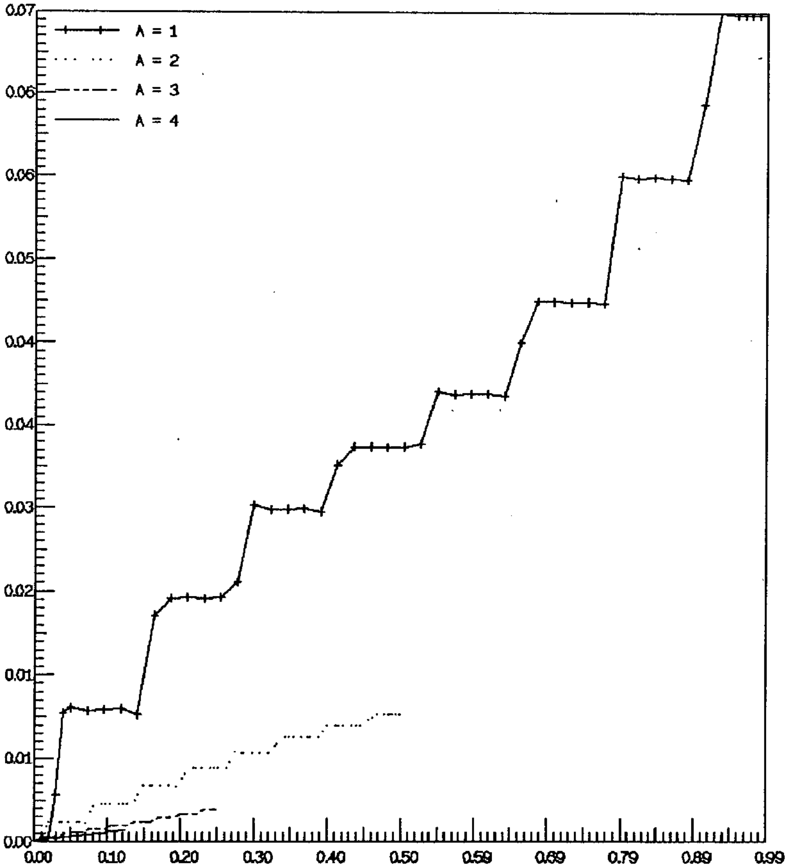

Figure 21. Cumulative heat flux vs. A for $Ra = 150$, $\phi = 0°$, $a = 0.4$, and $N = 8$.

presented, and is seen to be greater than that from a wavy surface. In the single wave case, this can be attributed to the manifestation of separated flow zones on the wavy wall, and in the multiple wave case, to the change in the pattern of the recirculation regions.

The streamlines and isotherms (Figure 12(a)–(f)) for varying phases, in the single wave case, are plotted for $Ra = 50$, $A = 1$, $a = 0.1$ with phase varying between 0 and 360°. As the phase varies from 0 to 360°, the reattachment point of the separated flow shifts from the bottom wall to the adjacent walls in the clockwise direction. Consequently, the counterflow zone emerging on the bottom wall grows in size covering the whole of the domain and leading to the manifestation of a cycle of uni- and bicellular flows. In the multiple wave case, the simulations have been carried out at $Ra = 100$, 200; $a = 0.4$, 0.7; $A = 1$. For $a = 0.4$ (Figure 13(a)–(f)), analogous to one wave case, a shift in the separation and reattachment points to the adjacent walls in the anticlockwise direction is observed. Also a change is observed in the dimensions of the cells. For $a = 0.7$ (Figure 14(a)–(h)) again a movement of separation and reattachment from right-to-left of the domain is observed. Clockwise and anticlockwise circulation zones are seen to alternatively emerge from the right-bottom corner of the domain and march into the domain with the shift in the separation and reattachment points. Consequently, a cycle of bicellular and tricellular prominent circulation zones are seen to manifest in the domain with the phase varying between 0 and 360°. Isotherms for varying phases are given in Figure 15(a)–(f). Isotherms close to the bottom wall are wavy in nature. Further, in accordance with the varying phase of the bottom wall, a change in the phase of the wavy isotherms is clearly noticed. Cumulative heat flux plots for this case study are presented in Figure 16. Figure 16(b) and (c), corresponding to the global heat flux in the single wave and multiple wave case, respectively, show that there is a periodic change in the heat flux with increasing phase.

Streamlines for the varying number of waves case are presented in Figure 17(a)–(d) for $N = 6$, 8, 10, 15 and $Ra = 150$, $A = 1$, and $\phi = 90°$. With the increase in the number of waves, a shift in the separation and reattachment points is observed. Consequently, a row–column array of circulation zones transform into just a row of circulation zones. From the isotherms presented in Figure 18, it is seen that with the increase in the number of waves, the wavy nature in the isotherms close to the bottom wall increase. Further, this wavy nature in isotherms extends deep into the domain. The cumulative heat flux plots for this case are presented in Figure 19. As the number of waves per unit length increase, a clear decrease in the heat flux into the system is observed.

Streamlines and isotherms corresponding to the flow and heat convection in porous enclosures with $A = 1$, 2, 4, 8 at $Ra = 150$, $\phi = 0°$, and $a = 0.4$ are presented in Figure 20(a)–(d). The plots in Figure 21 present the cumulative global heat flux. It is clearly seen that the global heat flux into the system decreases as the width of the cavity (l) is decreased, keeping the height (H) of the cavity fixed.

5. CONCLUSIONS

The effects of surface undulations on natural convection heat transfer in a Darcian fluid-saturated porous enclosure has been numerically analyzed using a FEM. The key observations of the study are

(a) Manifestations of separation zones on the wavy wall for values of Ra around 50 in the single wave case and around 25 in the case with six waves per unit length.

(b) Interesting flow features like the transformation of a unicellular flow to a multicellular flow with increasing Ra and the transformation of a row–column pattern of multicellular flow to a row pattern of multicellular flow with increasing N or with increasing a are observed.

(c) Multiple recirculation zones appear to hinder the heat flux into the system. This effect becomes profound if the separation and reattachment points where to lie on the wavy wall.

(d) Only marginal changes in heat flux is observed with increasing *Ra*.

(e) Either increasing the amplitude of the wavy wall or increasing the aspect ratio or the number of waves per unit length is found to decrease the heat flux into the system.

(f) A periodic change in the heat flux is observed with the phase varying between 0 and 360°.

APPENDIX A. NOMENCLATURE

a	amplitude of the wavy wall
e	typical element
g	gravitational constant
k	thermal conductivity
K	permeability
L	the length of the wavy wall
n	outward drawn unit normal to the wavy surface
N	number of waves considered per unit length
N_l	quadratic interpolation function
p	pressure
Q	global heat flux
Ra	Rayleigh number: $(Kg\beta\theta_w L)/v_\alpha$ based on the length of the wavy wall
$s(\xi)$	arc length of the wavy wall
T	temperature
u	horizontal velocity component
v	vertical velocity component
x, y	Cartesian co-ordinates

Greek letters

α	thermal diffusivity constant
β	thermal expansion coefficient
ϕ	phase of the wave
ψ	the dimensional stream function
Ψ	the non-dimensional stream function
θ	the non-dimensional temperature distribution
μ	viscosity of the fluid
ν	fluid kinematic viscosity
ξ	arc length variable
ρ	fluid density
Ω	the domain considered in the problem
Γ	the boundary of the domain

Subscripts

a	conditions at the ambient medium
w	evaluated at wall condition

REFERENCES

1. K. Vafai and P.C. Huang, 'Analysis of heat transfer regulation and modification employing intermittently emplaced porous cavities', *Trans. ASME*, **116**, 604–613 (1994).
2. B.K.C. Chan, C.M. Ivey and I.M. Bary, 'Natural convection in enclosed porous media with rectangular boundaries', *ASME J. Heat Transf.*, **2**, 21–27 (1970).
3. P.H. Holst and K. Aziz, 'A theoretical and experimental study of natural convection in a confined porous medium', *Can J. Chem. Eng.*, **50**, 232–241 (1972).
4. P.J. Burns, L.C. Chow and C.L. Tien, 'Convection in a vertical slot fitted with porous insulation', *Int. J. Heat Mass Transf.*, **20**, 919–926 (1976).
5. K.L. Walker and G.M. Homsy, 'Convection in a porous cavity', *J. Fluid Mech.*, **97**, 449–474 (1978).
6. A. Bejan and C.L. Tien, 'Natural convection in a horizontal porous medium subjected to an end-to-end temperature difference', *ASME J. Heat Transf.***, 100,** 191–198 (1978).
7. C.E. Hickox and D.K. Gartling, 'A numerical study of natural convection in horizontal porous layer subjected to an end-to-end temperature difference', *ASME J. Heat Transf.*, **103**, 797–802 (1981).
8. V. Prasad and F.A. Kulacki, 'Natural convection in a rectangular porous cavity with constant heat flux on one vertical wall', in J.V. Beck and L.S. Yao (eds), *ASME HTD*, **22**, 35–41 (1987).
9. P. Cheng, 'Heat transfer in geothermal systems', *Adv. Heat Transf.*, **14**, 1–105 (1978).
10. R. Bradean, D.D. Ingham, P.J. Heggs and I. Pop, 'Free convection fluid flow due to a periodically heate and cooled vertical flat plate embedded in a porous media', *Int. J. Heat Mass Transf.*, **39**, 2545–2557 (1996).
11. G. Hetsroni, A. Mosyok and L.P. Yarin, 'Effect of surface waves on heat transfer in natural and forced convection', *Int. J. Heat Mass Transf.*, **40**, 2219–2229 (1997).
12. D.A. Nield and A. Bejan, *Convection in Porous Media*, Springer, New York, 1992.
13. S.H. Bhavnani and A.E. Bergles, 'Natural convection heat transfer from sinusoidal wavy surface', *Wärme Stoffübertrag.*, **26**, 341–349 (1991).
14. D.A.S. Rees and I. Pop, 'A note on free convection along a vertical wavy surface in a porous medium', *J Heat Transf.*, **116**, 505–508 (1994).
15. D.A.S. Rees and I. Pop, 'Free convection induced by a horizontal wavy surface in a porous medium', *Fluid Dyn. Res.*, **14**, 151–166 (1994).
16. D.S. Riley, 'Steady two-dimensional thermal convection in vertical porous slot with spatially periodic boundary imperfections', *Int. J. Heat Mass Transf.*, **31**, 2365–2380 (1988).
17. S.G. Moulic and L.S. Yao, 'Natural convection along a vertical wavy surface with uniform heat flux', *J Heat Transf.*, **111**, 1106–1108 (1989).
18. L.S. Yao, 'Natural convection along a vertical wavy surface', *J Heat Transf.*, **105**, 465–468 (1983).
19. A. Watson and G. Poots, 'The effect of sinusoidal protrusions on laminar free convection between vertical walls', *J. Fluid Mech.*, **49**, 33–48 (1971).
20. K. Vajravelu and K.S. Sastri, 'Free convective heat transfer in a viscous incompressible fluid confined between a long vertical wall and parallel flat wall', *J. Fluid Mech.*, **86**, 365–383 (1978).
21. O.C. Zienkiesvicz and R.L. Taylor, *The Finite Element Method: Basic Formulation and Linear Problems*, 4th edn, McGraw-Hill, New York, 1989.